Overexpression of UCP4 in astrocytic mitochondria prevents multilevel dysfunctions in a mouse model of Alzheimer's disease

Nadia Rosenberg[1], Maria Reva[4], Francesca Binda[1], Leonardo Restivo[1], Pauline Depierre[1], Julien Puyal[1], Marc Briquet[1], Yann Bernardinelli[2], Anne-Bérengère Rocher[1], Henry Markram[4], and Jean-Yves Chatton[1,3*]

Supplementary Methods

Immunohistochemistry and confocal microscopy

Sagittal slices (30-50 µm) were obtained from PFA fixed brains prepared from WT and 3xTg naïve (8 months old) or AAVs injected mice (8-10 months old). Following one rinse in PBS, blocking was performed at room temperature for 3 hours with the following blocking solution: PBS supplemented with 10% serum (donkey or goat serum were used depending on the secondary antibodies; for MBP/RFP co-staining, a mix of goat and donkey serum, 10% each, was used) and 0.5 % Triton X-100. Slices were then incubated at 4°C with the appropriate primary antibodies diluted in blocking solution; incubation time varied between overnight (O/N) or for 2 days depending on the primary antibody used. Secondary antibody were used to a 1:500 final dilution in blocking solution with a 3 hours incubation time at room temperature. Nulcei were labelled at the end of immunostaining with Hoechst (1mg/ml) diluted 500 times in PBS (10-12 minutes of incubation).

   AAV-mediated transduction specificity was investigated by co-staining of mCherry or UCP4-HA tagged protein and markers specifically expressed in astrocytes, oligodendrocytes, microglia or neurons. Primary and secondary antibodies together with experimental conditions used are listed in **Table 1** below.

Table 1		
Primary Antibodies	*Specifications*	*Experimental Settings*
Mouse anti-GFAP	Sigma Aldrich, G3893	1:500 O/N at 4°C
Rat anti-MBP	Bio-Rad, MCA409S	1:500 O/N at 4°C
Goat anti-Iba1	Abcam, AB5076	1:500, O/N at 4°C
Mouse anti-Map2	Invitrogen, A21202	1:500, O/N at 4°C
Rabbit anti-RFP	Rockland, 600-401-379S	1:50, two days at 4°C
Rabbit anti-HA	Abcam 9110	1:500, O/N at 4° C
Secondary Antibodies	*Specifications*	*Experimental Settings*
Donkey anti-mouse Alexa Fluor 488	Invitrogen, A11055	1:500, 3 hours at RT
Goat anti-rat Alexa Fluor 488	Invitrogen, A11006	1:500, 3 hours at RT
Donkey anti-goat Alexa Fluor 488	Invitrogen, A11055	1:500, 3 hours at RT
Donkey anti-rabbit Alexa Fluor 790	Invitrogen, A11374	1:500, 3 hours at RT
Goat anti-rabbit Alexa Fluor 680	Invitrogen, A32734	1:500, 3 hours at RT

Astrogliosis was evaluated by GFAP immunostaining performed under the same experimental condition described above with the following primary and secondary antibodies: rabbit anti-GFAP (Dako, Z0334; 1:500) and donkey anti-rabbit Alexa Fluor Plus 488 (Invitrogen, A32790; 1:500).

Images were acquired with the Stellaris 8 confocal microscope (Leica) using a HC PL APO 63x/1.40 oil objective lens.

Image analysis: Images were analyzed with ImageJ (Rasband WS, 1997-2018) and astrocytes were reconstructed with the SNT tool; z-stacks contrast was manually adjusted to clearly visualized astrocytes processes that were traced starting from the center of the nucleus and followed on the adjacent z-planes (Tavares et al., 2017).

Images processing: To improve image display and obtain a better representation of the results, the contrast of images included in Figures S2-6 and Figure S8 was enhanced by normalization with a 0.35% pixels saturation.

Immunoblotting

The hippocampi of 8-10 months aged male AAV-mCherry-UCP4 or AAV-mCherry injected 3xTg-AD mice were dissected out and collected in lysis buffer (20 mM HEPES, pH 7.4, 10 mM NaCl, 3mM $MgCl_2$, 2.5 mM EGTA, 0.1 mM dithiothreitol, 50 mM NaF, 1mM Na_3Vo_4, 1% Triton X-100 and a protease inhibitor cocktail (Sigma, #11873580001)). Tissues were manually grinded and sonicated and protein concentration was determined by Bradford assay (Bio-Rad, #5000006).

Proteins (40 µg) were separated on SDS-PAGE (10% polyacrylamide (National Diagnostics, EC-890)) gels and transferred on nitrocellulose membrane (Bio-rad, #1620115). Membranes were then blocked with blocking buffer (BSA 2% (Sigma, A6003), 0.1M PBS) at RT for about 1 hour and incubated in primary antibody prepared in BSA 2% buffer at 4°C overnight. The following primary antibodies were used for protein immunodetection: mouse monoclonal anti-actin (ACT) from Millipore (#MA511869, 1/2000), rabbit polyclonal anti-HA tag from abcam (#ab9110, 1/1000). The membranes were washed with 0.1M PBS Tween 0.1% and incubated for 1 hour at RT in secondary antibody. Following secondary antibodies prepared in BSA 2% buffer were used (at 1/10'000): goat anti-mouse IgG (H+L) DyLight 680 Conjugate (Cell Signaling, #5470S) and mouse anti-rabbit IgG DyLight 800 (Rockland, #18-4516-32). After final washes, protein bands were visualized with Odyssey infrared imaging system (LI-CORE, NE, USA).

Real-Time qRT-PCR

The hippocampi of 8-10 months aged male AAV-mCherry-UCP4 and AAV-mCherry injected 3xTg-AD mice, or WT and 3xTg-AD mice, were dissected out and total mRNA was extracted using the RNeasy Mini Kit (Quiagen, #74104). For cDNA synthesis, reverse transcriptase was carried out with High-Capacity cDNA Reverse Transcription Kit (Applied Biosystems, #4368814) from 1.5 µg of total RNA. Quantitative PCR amplification were performed with Power SYBR Green PCR Master mix (BioRad, #170-8880) and 200 nM primer pair sequences (UCP4: 5'-CTC AGA GCC AAC CGA ATA GC-3', 5'-GGC TGA CAG ATG CAA CAG AA-3'; GAPDH: 5′-CCCCCAATGTGTCCGTCGTG-3′ and 5′-TAGCCCAAGATGCCCTTCAGT-3′ (Microsynth)). Samples were run in triplicate. Values were normalized with the housekeeping gene GAPDH and expressed as a percentage as specified in the figure.
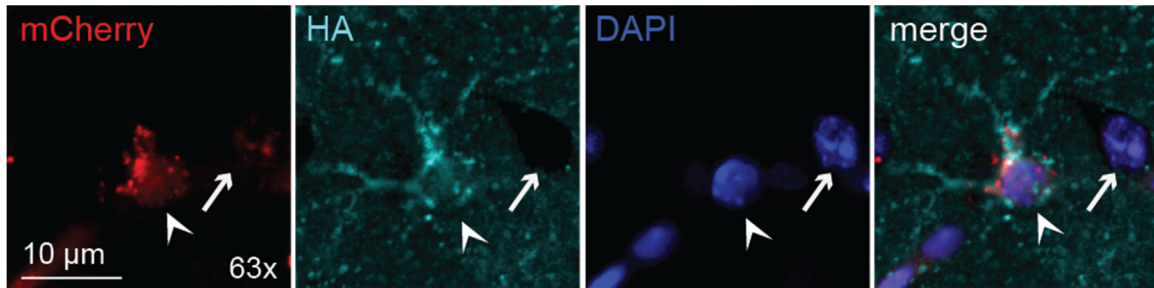
Supplementary Figures

Figure S1. UCP4 expression at 4 months post-injection. Confocal image of an astrocyte and a neuron in the CA1 region (highlighted with a white arrowhead and a white small arrow, respectively) showing HA-tag (cyan) fluorescent immunostaining and mCherry (red) plus DAPI (blue) revealing specific HA-tag expression in astrocyte only at 4 months in WT mice.
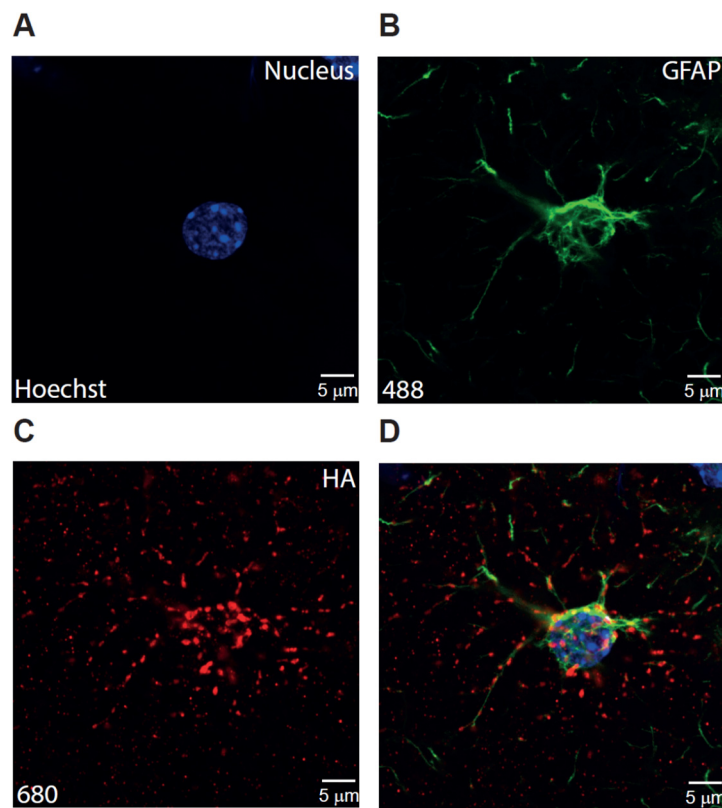

Figure S2. Astrocytic expression of exogenous HA tagged UCP4 at 8 months post-injection. Exogenous UCP4 is expressed at 8 months after rAAVs injection as shown by HA tag immunostaining (C) and it localized (D) to GFAP- stained (B) astrocytes. Figure panels show confocal images (z-stack maximum projection) of an astrocyte in the CA1 hippocampal region of a 3xTg mouse injected with UCP4-HA.
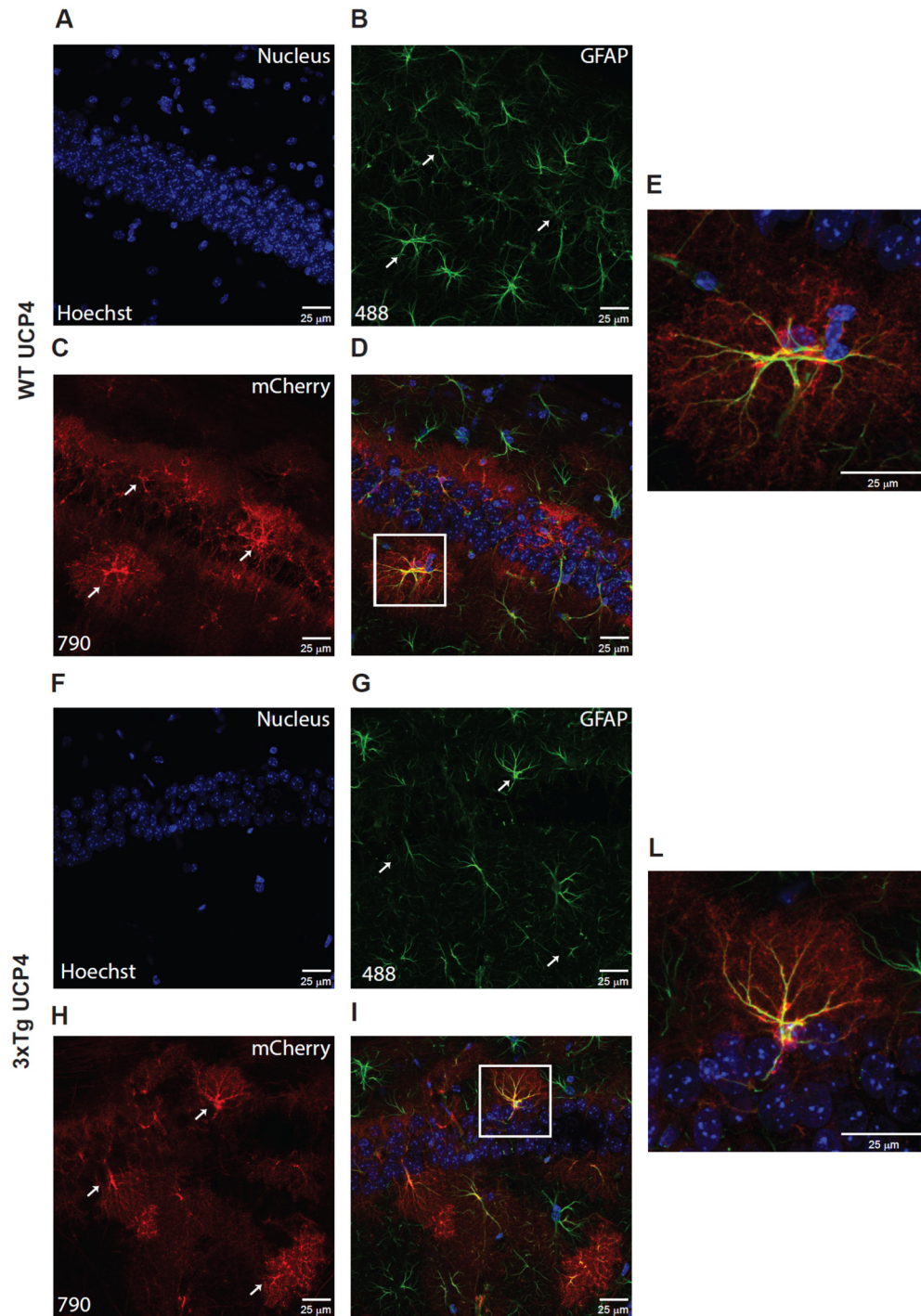
Figure S3. Long-term expression of recombinant proteins retains specificity. mCherry immunostaining (red, C and H, white arrows) in the CA1 hippocampal region of UCP4-injected WT (A-E) and 3xTg (F-L) mice revealed expression of the fluorescent protein at 6-8 months post-injection; expression was localized to astrocytes (D and I) as shown by GFAP staining (green, B and G, white arrows). mCherry and GFAP colocalization is visible in panels E and L showing the enlargement of the astrocytes indicated by the white squares in panel D and I respectively. Confocal images, z-stack maximum projections are showed in the figure panels.
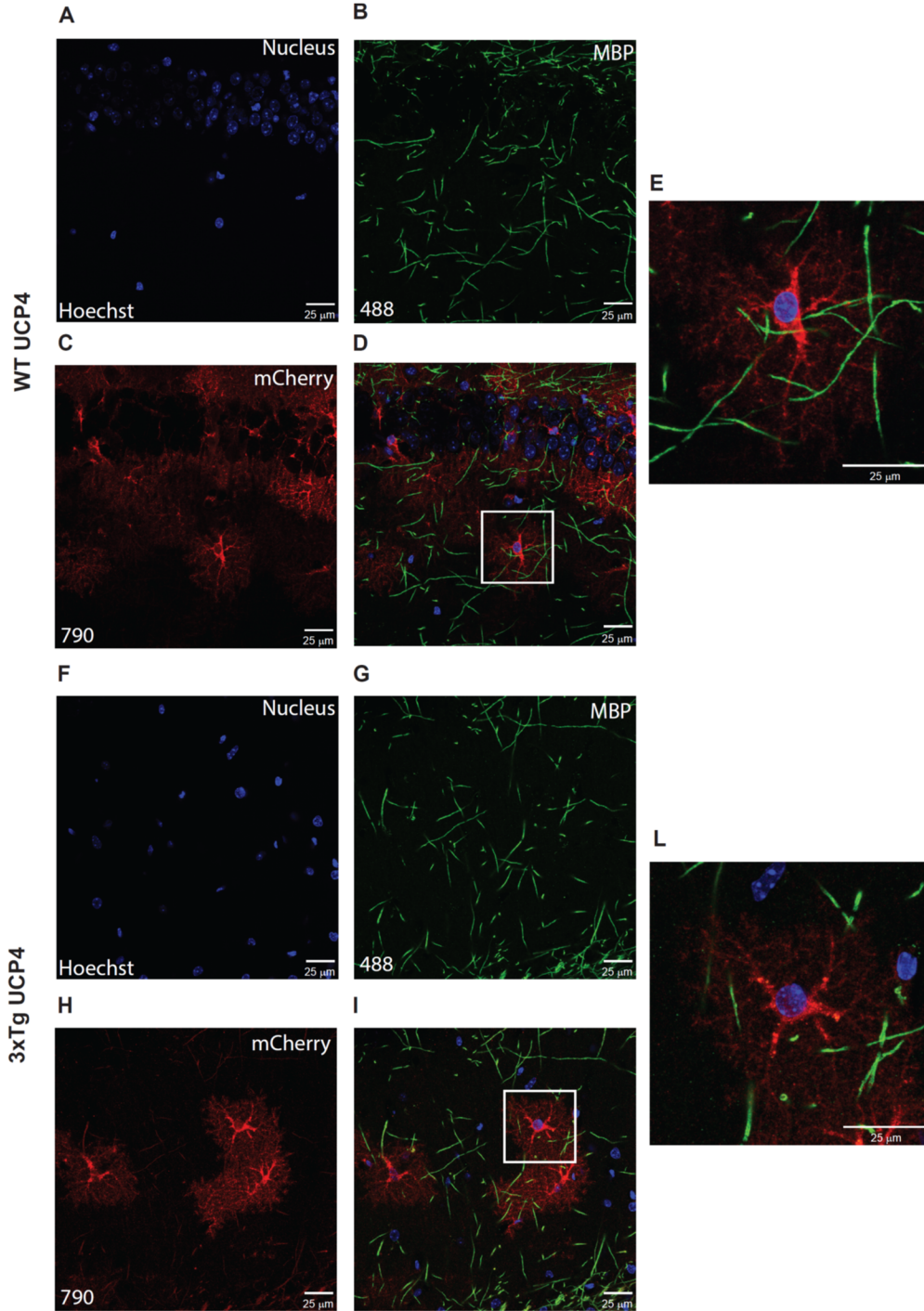
Figure S4. Recombinant proteins are not expressed in oligodendrocytes. Hippocampal slices from UCP4-injected WT and 3xTg mice (6-8 months after injection) were immunostained for the oligodendrocyte-specific marker MBP (green, B and G) and mCherry (red, C and H); a not-overlapping expression was detected (D and I) in both genetic backgrounds. Lacking of co-localization is visible in panels E and L showing the enlargement of the astrocytes indicated by the white squares in panel D and I respectively. Confocal images, z-stack maximum projections are shown in the figure panels.
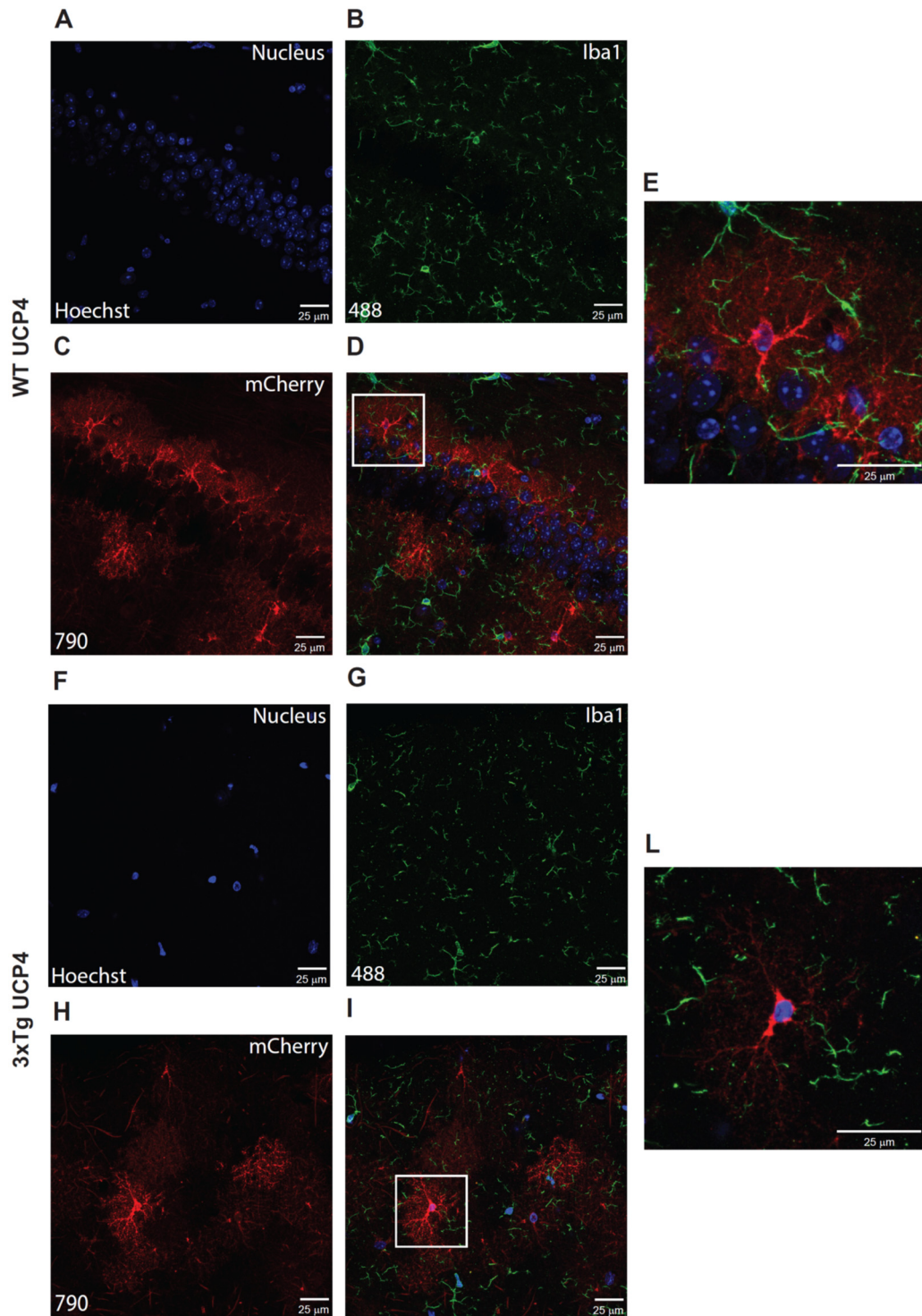
Figure S5. Recombinant proteins are not expressed in microglia. Immunostaining for the microglia-specific marker Iba1 (green, B and G) and mCherry (red, C and H) showed uncorrelated expression of the two proteins in both WT (D) and 3xTg (I) UCP4-injected mice (6-8 months after injection). Lacking of co-localization is visible in panels E and L showing the enlargement of the astrocytes indicated by the white squares in panel D and I respectively. Confocal images, z-stack maximum projections are shown in the figure panels.
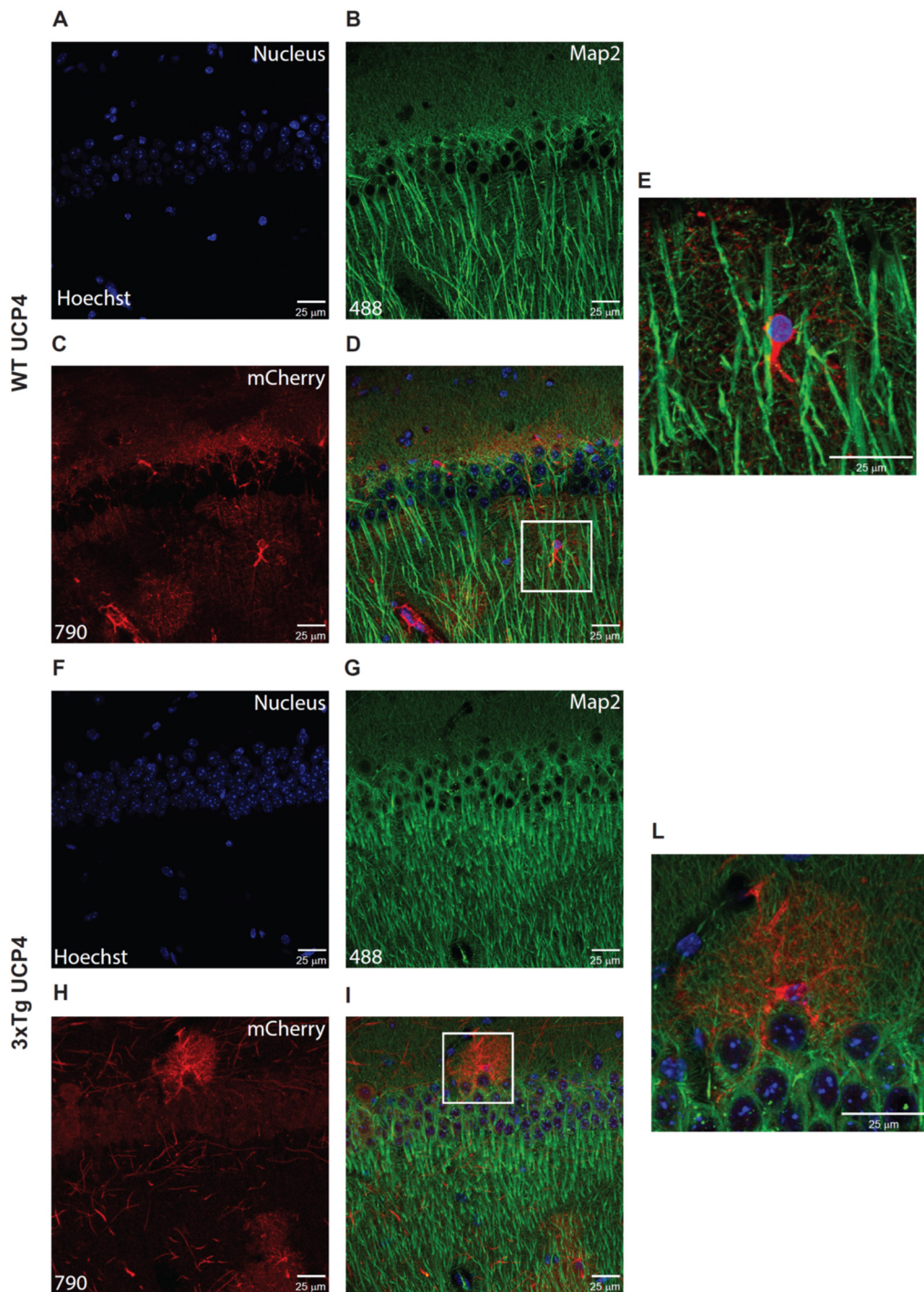
Figure S6. Recombinant proteins are not expressed in neurons. Neurons stained for the specific neuronal marker Map2 (green, B and G) showed no mCherry expression (red, C and H) in both WT (D) and 3xTg (I) UCP4-injected mice (6-8 months after injection). Lacking of co-localization is visible in panels E and L showing the enlargement of the astrocytes indicated by the white squares in panel D and I respectively. Confocal images, z-stack maximum projections are shown in the figure panels.
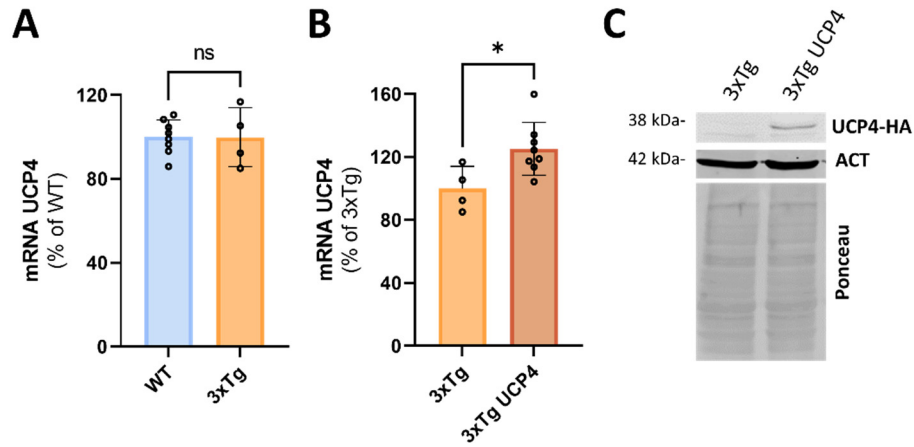
Figure S7. UCP4 expression in naïve and injected mice . (**A**) Real-Time qRT-PCR revealed similar UCP4 mRNA levels in WT and 3xTg-AD male mice at 8-10 months of age (WT: 100.0 ± 2.87%, n=8; 3xTg-AD: 99.88 ± 7.03%, n=4; unpaired t-test, two replicates per animal, p=0.958). (**B**) Real-Time qRT-PCR showed that AAV-mediated overexpression of UCP4 in 3xTg-AD animals significantly increased UCP4 mRNA levels (3xTg-AD: 100.0 ± 7.04%, n=4; 3xTg-AD UCP4: 125.3 ± 5.94%, n=8, unpaired T-test, two replicates per animal, p=0.0276). (**C**) Representative immunoblot against HA showing that UCP4-HA is detected in hippocampus of AAV9-mCherry-UCP4 compared to AAV9-mCherry 3xTg-AD injected mice. Values are expressed as mean ± SD.
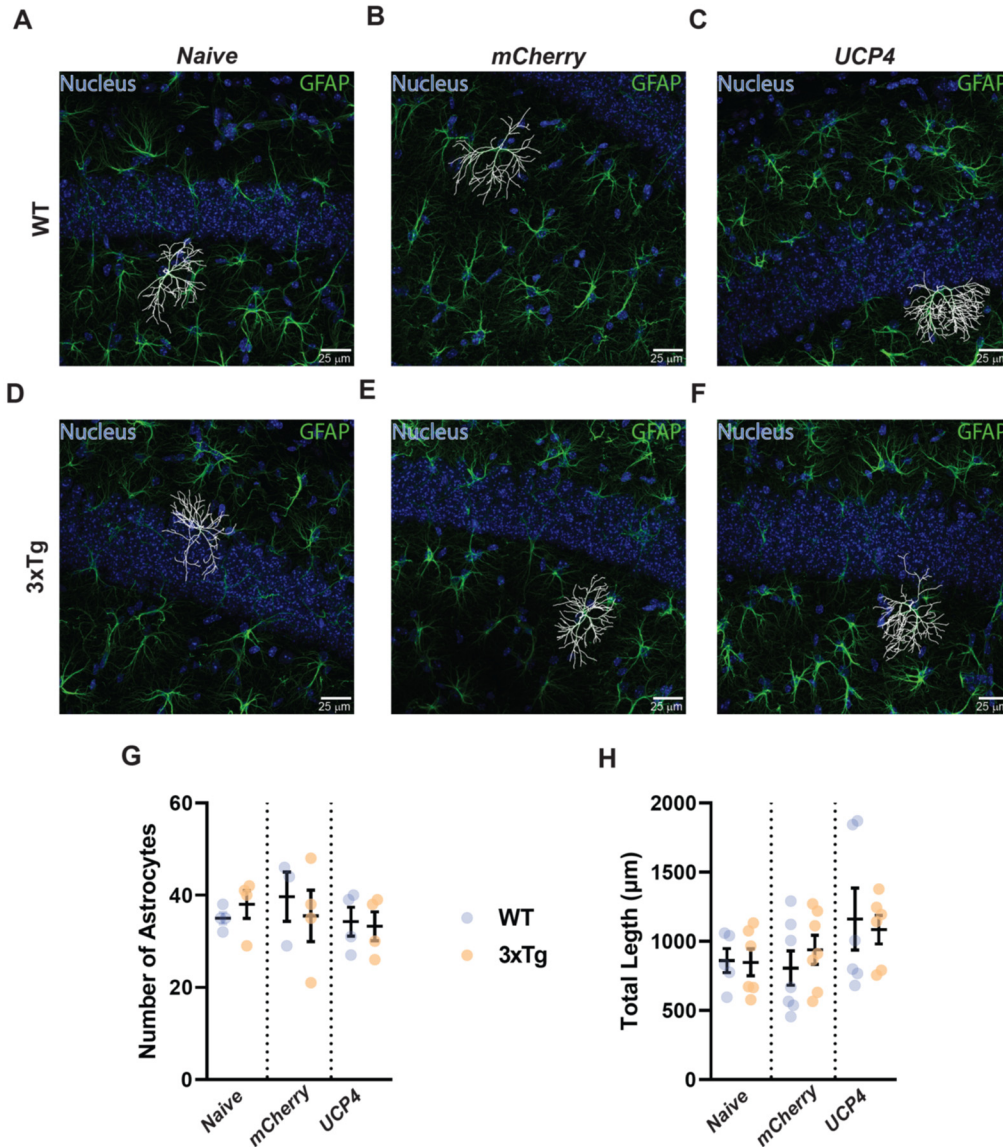
Figure S8. Long-term expression of recombinant proteins have no significant impact on astrocytes morphology in old mice. Astrocytes morphology in the CA1 hippocampal region of old WT and 3xTg mice not injected (B and G), injected with mCherry (B and E) and UCP4 injected was characterized by tracing of GFAP-stained astrocytic projections along z-planes of confocal z-stacks (representative reconstructed astrocytes are show in white in the images) and determination of the total projections length (H, mean ± SEM, N = 1 mouse/condition, n = 3-4 slices/mouse analyzed). Statistical analysis revealed no statistically significant differences among groups (Two-way Anova, interaction P = 0.71, genotype P = 0.89, treatments P = 0.1; Dunnett's multiple comparisons test: WT, naïve vs mCherry P = 0.94, naïve vs UCP4 P = 0.24; 3xTg, naïve vs mCherry P = 0.84, naïve vs UCP4 P = 0.36). Quantification of the number of astrocytes/slice under each experimental conditions (G) showed no statistically significant difference among groups (Two-way Anova, interaction P = 0.65, genotype P = 0.82, treatments P = 0.58; Dunnett's multiple comparisons test: WT, naïve vs mCherry P = 0.63, naïve vs UCP4 P = 0.98; 3xTg, naïve vs mCherry P = 0.85, naïve vs UCP4 P = 0.57). Confocal images, z-stack maximum projections are shown in the figure panels.
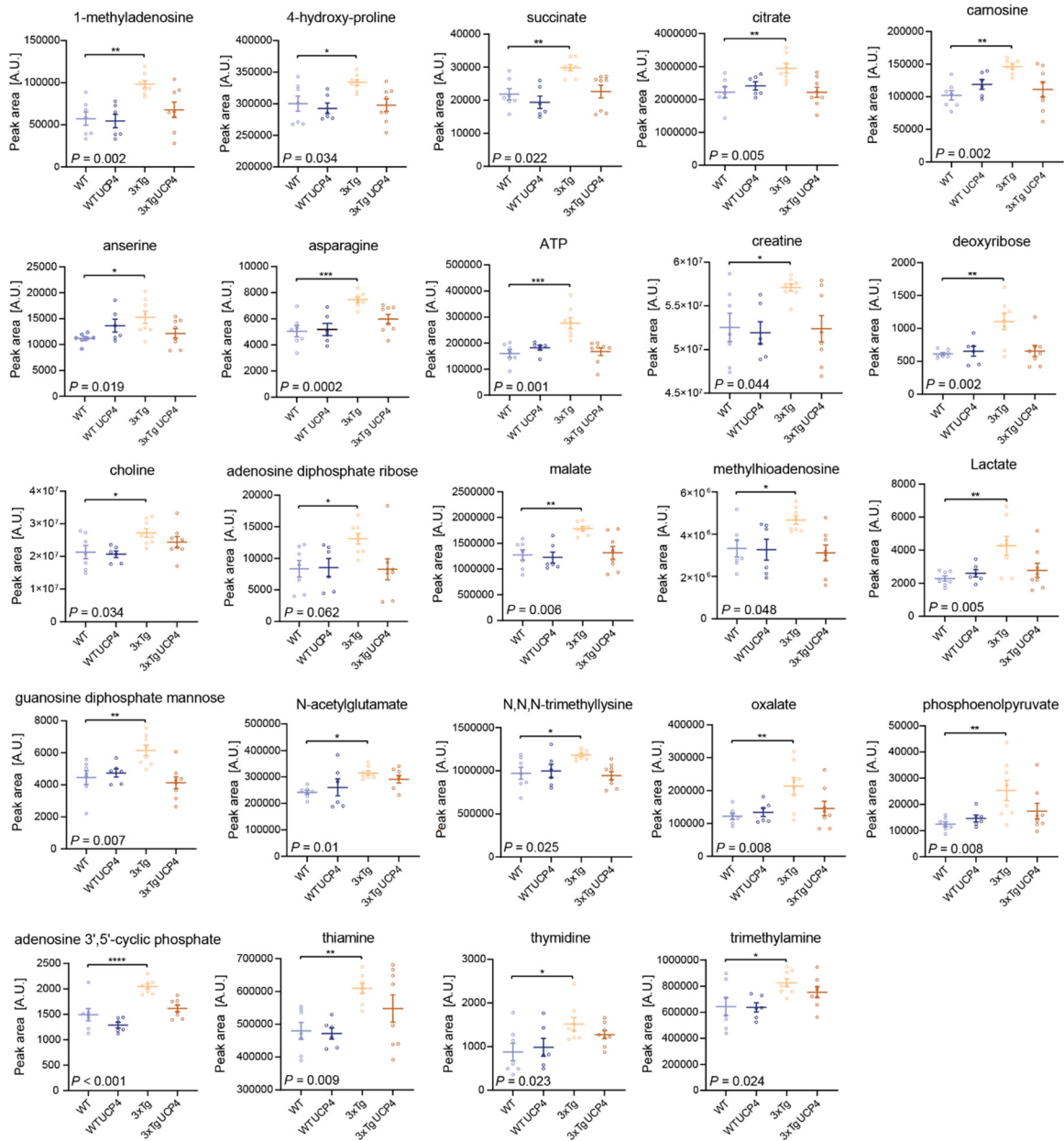
Figure S9. Metabolites that are altered in 3xTg mice but which are maintained to WT levels by overexpression of UCP4. Plots of selected metabolites comparing hippocampal levels in WT (n=7), WT UCP4 (n=6), 3xTg (n=8), and 3xTg UCP4 (n=8) mice. Each dot represents a different specimen. One-way ANOVA followed by Tukey's post hoc test was performed, except for succinate, ATP, adenosine diphosphate ribose, methylhioadenosine and phosphoenolpyruvate a Kruskal-Wallis followed by a Dunn's post hoc test was done. *P <0.05; **P <0.01; ***P <0.001; ****P <0.0001.
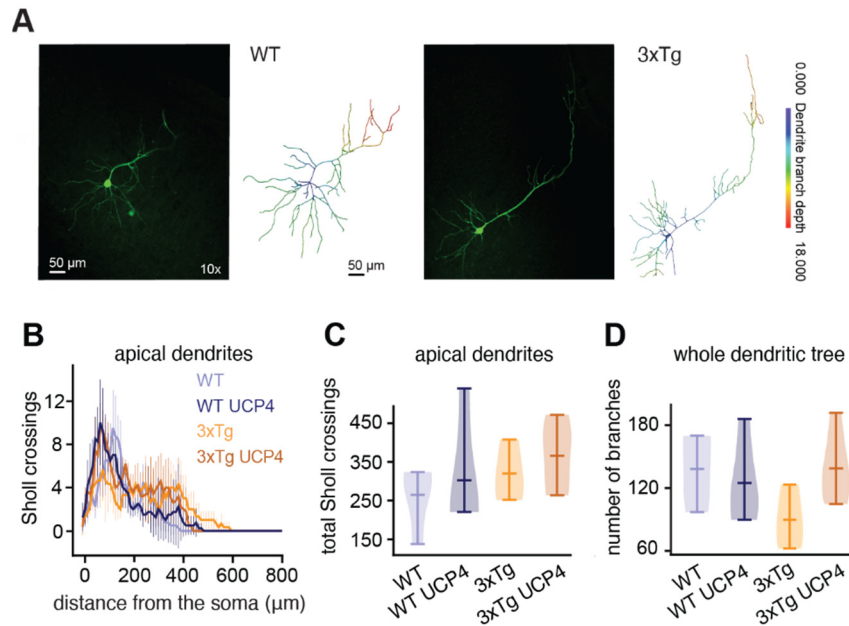
Figure S10. Sholl profiles and morphometrics of apical dendrites. (**A**) Representative confocal images of WT (left) and 3xTg (right) subicular neurons filled with biocytin. The respective 3D reconstructions are shown with color-coded dendrite branch depth. (**B**) Sholl profile for each group, calculated using 5 µm increments (WT: n = 4, WT UCP4: n = 4, 3xTg: n = 3, 3xTg UCP4: n = 5), where n is the number of reconstructed neuronal morphologies from the 3D models coming from 16 different mice. (**C**) Total number of Sholl crossing of apical dendrites for each group. No significant statistical difference was found between the groups. (**D**) Total number of dendritic branches for each group, calculated for each morphology. In **C** and **D** a non-parametric bootstrapping test was performed: no significant statistical difference was found between the groups. Same n as **B**. Bars on violin plots are mean ± CI.
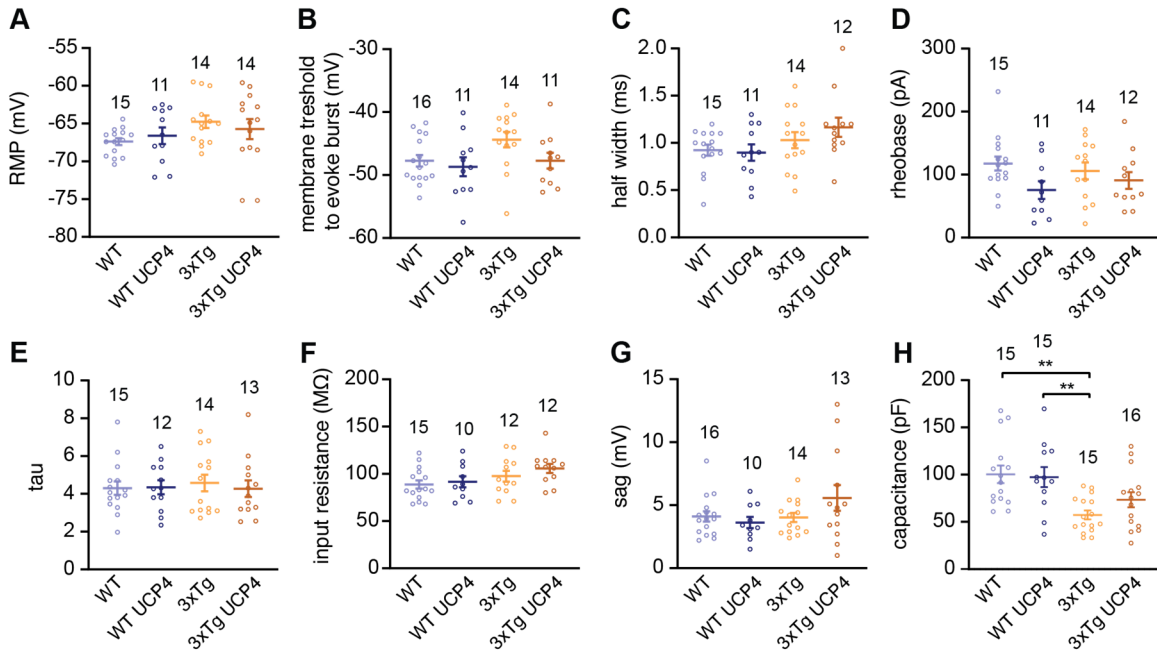
Figure S11. Intrinsic electrophysiological properties of subicular neurons are not altered by viral constructs. Patch-clamp recordings of subicular neurons show no differences in intracellular properties, namely (**A**) resting membrane potential (RMP), (**B**) threshold to evoke burst, (**C**) AP half-width, (**D**) rheobase, (**E**) decay (tau), (**F**) input resistance, and (**G**) sag among groups, except for (**H**) capacitance. The numbers above each data set represent the number of neurons patched coming from at least 10 different mice per group. In **A**-**D**, **F,** and **G** a one-way ANOVA followed by Tukey's *post hoc* test was performed, and in **E** and **H** a Kruskal-Wallis followed by a Dunn's post hoc test was done. Error bars are mean ± SEM. **P < 0.01.
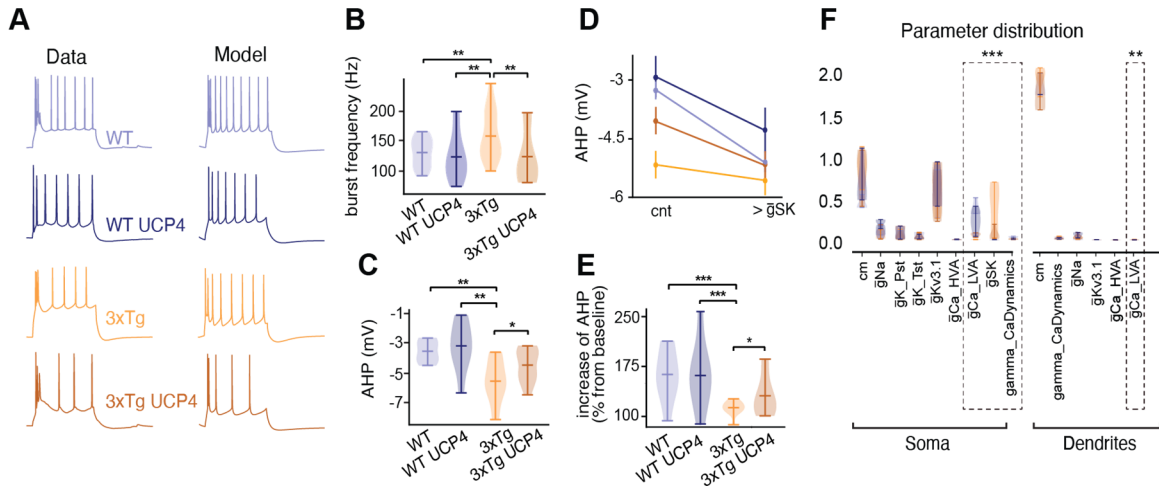
Figure S12. Generation and validation of subicular neuron models. (**A**) Example traces of current clamp recordings (*Data*) and corresponding traces from neuronal models (*Model*). (**B**) Violin plot of burst frequencies in responses to simulated 200, 300 and 450pA current injections. Several models were considered for each group (WT: n=5, WT UCP4: n=5, 3xTg: n=7, 3xTg UPC4: n=5). (**C**) Violin plot of AHP in responses to pooled 200 and 450pA current injections. (**D**) AHP in control condition (cnt, same as in C), compared to a manually increased SK conductance (>ḡSK), across pooled models' responses to 200 and 450pA current injections. (**E**) Violin plot of AHP with increased ḡSK shown as percentage of control AHP amplitude. (**F**) Distribution of model parameters compared across groups of models (same color scheme as in (**A**)) Scale on the left: absolute value. Those include unitary capacitance (cm), sodium channel conductance (ḡNa), persistent potassium conductance (ḡK_Pst), transient potassium conductance (ḡK_Tst), potassium voltage gated channel conductance (ḡKv3.1) (Rudy & McBain, 2001) (Rudy & McBain, 2001), high voltage activated calcium channels conductance (ḡCa_HVA), low voltage activated calcium channel conductance (ḡCa_LVA) (Perez-Reyes, 2003) (Perez-Reyes, 2003), ḡSK, and gamma_CaDynamics, corresponding to the percentage of free intracellular calcium levels. Significant statistical difference between groups are highlighted by the dashed line rectangles. Scale on the left: absolute value. Bars on violin plots are mean ± CI. In (**B**), (**C**) and (**E**), nonparametric bootstrap test was performed. In (**D**) error bars represent mean ± SEM. In (**F**), Kruskal-Wallis, followed by a *post hoc* Bonferroni correction test was performed (somatic ḡCa_LVA (maximum conductance of low threshold calcium channels; KS: P = 3.9e-4, post hoc Bonferroni correction: 3xTg vs WT: P = 1.4e-7, 3xTg vs WT UCP4: P = 2.2e-5, 3xTg vs 3xTg UCP4: P = 1.2e-3, WT vs 3xTG-UCP4: P = 2e-3, alpha = 0.01), somatic ḡSK (maximum conductance of SK channel, KS: P = 4.5e-4, post hoc Bonferroni correction 3xTg vs WT: P = 2e-6, 3xTg vs WT UCP4: P = 5e-6, WT vs 3xTg UCP4: P = 4e-4, alpha = 0.01), somatic gamma_CaDynamics (percentage of free intracellular calcium; KS P = 5e-4, post hoc Bonferroni correction 3xTg vs WT: P = 1e-4, WT vs 3xTg UCP4 P = 8e-6, WT UCP4 vs 3xTg UCP4 P = 1.3e-4, alpha = 0.01) and apical ḡCa_LVA (KS: P = 2.9e-4, post hoc Bonferroni correction 3xTg vs WT: P = 5e-4, 3xTg vs WT UCP4 P = 3e 2, WT UCP4 vs 3xTg alpha = 0.01). *P < 0.05; **P < 0.01; ***P < 0.001. Bars on violin plots are mean ± CI.
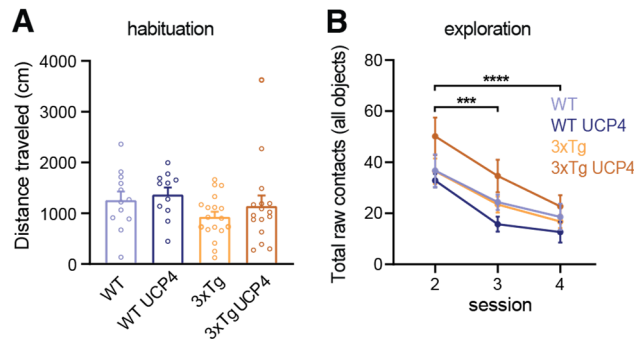
Figure S13. Viral vectors do not affect overall locomotory behavior. (**A**) Distance traveled by the mice during the habituation trial. (WT: n=12, WT UCP4: 11, 3xTg: n=18, 3xTg UCP4: n=16). (**B**) Overall number of contacts with the 3 objects across sessions. Data are the average contact number with objects (same n per group as in **A**). In (**A**) a Kruskal-Wallis followed by a Dunn's test was performed. In (**B**) a two-way ANOVA followed by Tukey's *post hoc* test was performed, and the error bars are mean ± SEM. ***$P < 0.001$; ****$P < 0.0001$.

Supplementary References

Perez-Reyes, E. (2003). Molecular physiology of low-voltage-activated t-type calcium channels. *Physiological Reviews, 83*(1), 117-161. doi:10.1152/physrev.00018.2002

Rasband, W.S., ImageJ, U. S. National Institutes of Health, Bethesda, Maryland, USA, https://imagej.nih.gov/ij/, 1997-2018.

Rudy, B., & McBain, C. J. (2001). Kv3 channels: voltage-gated K+ channels designed for high-frequency repetitive firing. *Trends in Neurosciences, 24*(9), 517-526. doi:10.1016/s0166-2236(00)01892-0

Tavares, G., Martins, M., Correia, J. S., Sardinha, V. M., Guerra-Gomes, S., das Neves, S. P., . . . Oliveira, J. F. (2017). Employing an open-source tool to assess astrocyte tridimensional structure. *Brain Structure & Function, 222*(4), 1989-1999. doi:10.1007/s00429-016-1316-8